Molecular dynamics simulation of strong shock waves propagating in dense deuterium, taking into consideration effects of excited electrons

Hao Liu,[1] Yin Zhang,[2] Wei Kang,[1,3,*] Ping Zhang,[1,4] Huiling Duan,[1,2] and X. T. He[1,3,4,†]

[1]*HEDPS, Center for Applied Physics and Technology, College of Engineering, Peking University, Beijing 100871, China*

[2]*Department of Mechanics and Engineering Science, College of Engineering, Peking University, Beijing 100871, China*

[3]*Collaborative Innovation Center of IFSA (CICIFSA), Shanghai Jiao Tong University, Shanghai 200240, China*

[4]*Institute of Applied Physics and Computational Mathematics, Beijing 100088, China*

(Received 21 November 2016; published 1 February 2017)

We present a molecular dynamics simulation of shock waves propagating in dense deuterium with the electron force field method [J. T. Su and W. A. Goddard, Phys. Rev. Lett. **99**, 185003 (2007)], which explicitly takes the excitation of electrons into consideration. Nonequilibrium features associated with the excitation of electrons are systematically investigated. We show that chemical bonds in D_2 molecules lead to a more complicated shock wave structure near the shock front, compared with the results of classical molecular dynamics simulation. Charge separation can bring about accumulation of net charges on large scales, instead of the formation of a localized dipole layer, which might cause extra energy for the shock wave to propagate. In addition, the simulations also display that molecular dissociation at the shock front is the major factor that accounts for the "bump" structure in the principal Hugoniot. These results could help to build a more realistic picture of shock wave propagation in fuel materials commonly used in the inertial confinement fusion.

DOI: 10.1103/PhysRevE.95.023201

I. INTRODUCTION

Inertial confinement fusion (ICF) [1–3] is an effective way to generate energy. The method requires one to compress the fusion fuel, composed of hydrogen isotopes deuterium (D) and tritium (T), into an extreme state over 1000 times the solid density. This high-density condition is difficult to attain through static compressions with current techniques. Dynamical approaches are commonly used instead, in which shock waves driven by high-power lasers or explosives are employed to compress the fuel. Therefore, understanding how strong shock waves compress the fuel is a necessity in the study of ICF.

Much effort has been devoted to understanding the structure of strong shock waves in various materials [4–13]. Early theoretical works based on the Navier-Stokes equations [4,9] and the Boltzmann equation [5,14] provide a basic physical picture of shock waves in fluids. With the development of computational techniques, in particular with the advent of efficient numerical hydrodynamic methods and codes [15,16], it is possible to show the structure of shock waves with increasing details and under complicated conditions close to those experienced by the fuel material. For strong shock waves, the underlying local thermal equilibrium (LTE) assumption in theoretical investigations can be partially removed by the classical molecular dynamics (MD) method [6,8,11,17]. It takes kinetic effects of atoms into account, and thus gives a better description of the shock wave structure. Classical MD simulations performed at various levels of technical sophistication [10,11,18,19] have shown that there are highly nonequilibrium behaviors, including shock induced phase transitions [20,21], and molecular dissociation [19,22], in the region near the shock front. These findings have stimulated further development of shock wave theories [13,18,23–25].

Unlike in weak shock compressions, where the material properties are mainly determined by degenerate electrons, it has been well recognized [4,26,27] that the excitation of electrons is an essential factor that has to be taken into account in the compression of fuel materials. The excitation appears as, for example, strong ionization and charge separation near the shock front at high impact velocity. It becomes significant when the downstream temperature of the shock wave rises to above 5 eV, which is typical in the implosion process of ICF.

Although there are a few of methods [28–30] that can take the excitation of electrons into consideration, the actual choice of methodology is quite limited as long as nonequilibrium features of both electrons and ions are concerned. Methods that explicitly depend on the electronic temperature, e.g., the finite-temperature density functional theory (time-independent version) [30], have to be excluded from the list, because local temperature has been demonstrated in previous works [11,17,24] not well defined in the highly nonequilibrium region near the shock front.

The nonequilibrium feature of electrons can be captured when the time-dependent dynamics of electrons is included faithfully. However, preceding attempts to deal with this on the level of the time-dependent density functional theory (TD-DFT) [31–33] have shown that this approach is extremely computationally costly. Practically, it is only capable of including tens of atoms in the calculation, which is far less than the required number of atoms to describe the propagation of shock waves. So, it is more realistic to use some simplified version of time-dependent electronic dynamics, e.g., the so-called wave-packet molecular dynamics (WPMD) method [26,34–36], which approximates electronic wave functions as Gaussian wave packets and describes the dynamics of electrons through the average positions and smearings (sizes) of the wave packets.

*weikang@pku.edu.cn

†xthe@iapcm.ac.cn

In this work, the excitation of electrons is described by the electron force field (eFF) method [26,37–39], which is a further development of the WPMD method. In addition to the Gaussian wave-packet approximation to electronic wave functions, the eFF method provides a simplified parametrization with improved accuracy to the Pauli's exclusion force between electrons of the same spin, which is a necessary part in the description of electronic structures, e.g., the shell structure and chemical bonds. Further studies of fuel materials in the equilibrium states [26,37] have shown that this method can also be applied to materials under high energy density conditions [40] typical in the ICF experiments. This encourages us to employ it in the investigation of dynamical structures of shock front.

We present a molecular dynamics simulation of shock waves propagating in deuterium with the eFF method, where nonequilibrium features associated with the excitation of electrons are addressed. We show with the simulation that chemical bonds in D_2 molecules lead to a more complicated shock wave structure near the shock front. Charge separation at the shock front brings about accumulation of net charges on large scales, instead of the formation of a localized dipole layer, which may cause extra energy for the shock wave to propagate. In addition, the simulation also displays that molecular dissociation at the shock front is the major factor that accounts for the "bump" structure in the principal Hugoniot.

The rest of the article is organized as follows. The theoretical description and computational details of the eFF method are presented in Sec. II. Section III discusses the main results and Sec. IV concludes the entire work with a short summary.

II. METHODOLOGY AND COMPUTATIONAL DETAILS

The propagation of shock waves in deuterium is simulated with a combination of classical molecular dynamics method for ions and the eFF method for electrons. The interaction between ions and electrons are assumed to be adiabatic and forces between them are calculated through the Ehrenfest's theorem [41]. Electron-electron interaction is described by the eFF method proposed by Su and Goddard [26]. In the eFF method, the electronic wave function of each electron is approximately described by a Gaussian wave packet,

$$\Psi(\mathbf{r}) \propto \exp\left\{-\left[\frac{1}{s^2}-\frac{2p_s}{s}\frac{i}{\hbar}\right](\mathbf{r}-\mathbf{x})^2-\frac{i}{\hbar}\mathbf{p_x}\cdot\mathbf{r}\right\}, \quad (1)$$

where s represents the smearing (the size) of the wave packet, $\mathbf{x}$ is the average position of the wave packet, and p_s is the conjugate momentum of s. The semiclassical equations of motion for $\mathbf{x}$ and s are derived [42] by inserting the wave-packet approximation into the time-dependent Schrödinger equation, which leads to

$$\begin{aligned} \dot{\mathbf{p}}_\mathbf{x} &= -\frac{\partial V}{\partial \mathbf{x}}, \qquad \mathbf{p_x} = m_e\dot{\mathbf{x}}, \\ \dot{p}_s &= -\frac{\partial V}{\partial s}, \qquad p_s = \frac{3}{4}m_e\dot{s}, \end{aligned} \quad (2)$$

with $V = V_{ii} + V_{ie} + V_{ee} + E_{KE} + E_{PR}$. The time derivatives are denoted as dots overhead in Eq. (2). Here, V_{ii}, V_{ee}, and V_{ie} represent the ion-ion, electron-electron, and ion-electron interactions, respectively. E_{KE} and E_{PR} are the kinetic energy of the Gaussian wave packet and Pauli repulsion energy, which account for quantum mechanical effects of electrons. There are several sophisticated constructions for the expression of E_{PR}. In our calculation, we use the simplest one following Ref. [37].

All simulations are performed using the eFF implementation included in the molecular dynamics code LAMMPS [43]. The mass of a real electron is 0.00055 amu, while in our simulation the electron mass is set as $m_e = 0.01$ amu to perform the simulation with a relatively large time step $\Delta t = 0.01$ fs. Simulations with $m_e = 0.1$ are also carried out to illustrate the mass effect of electrons. Note that the m_e here is different from that used in Su and Goddard's original work, in which m_e is set as 1 amu [37]. It is reasonable to set $m_e = 1$ amu for systems at equilibrium, but in a dynamical simulation, it would be better to give electrons a smaller mass to capture the charge separation effect.

The simulation box has a size of $102.271 \times 102.271 \times 33\,749.5$ bohr, corresponding to the length along the x, y, and z axes, respectively. Initially, the simulation box is filled with 2 640 000 deuterium atoms and 2 640 000 electrons. The initial Wigner-Seitz radius of deuterium atoms is $r_s = 3.1722$ bohr, corresponding to $\rho_0 = 0.169$ g/cc. Before shock waves propagate, the entire system is thermalized to a liquid state of deuterium at $T_0 = 20$ K and $P_0 = 27$ MPa.

Periodic boundary conditions along the x and y axes are assumed throughout the simulation. A reflective wall moving at a constant speed v_p is used as the piston to drive the shock wave. The piston is placed at one end of the z axis so that the shock wave travels along the positive z direction. At the other end of the z axis, a fixed reflective wall is used to keep the deuterium atoms in the simulation box. Simulations are terminated before fast electrons hit the reflective wall in order to remove its influence on the shock wave structure. The piston speed v_p varies from 20 km/s to 70 km/s. The corresponding shock velocity v_s is ranged from 25.2 km/s to 88.5 km/s, as summarized in Table I.

The cutoff for pair interactions is 10 bohr, which is more than 3 times the Wigner-Seitz radius of deuterium atoms. It takes all the interactions of the nearest and the next-nearest neighbors into consideration. The value of the cutoff is a tradeoff between computational efficiency and the size of simulation. Neglecting the long-range part of the Coulomb

TABLE I. Shock wave parameters extracted from the MD simulations, where v_p is the piston velocity, v_s is the shock wave speed, and η is the compression ratio, which is defined as the ratio of mass density in the downstream and upstream region. T and P are temperature and total pressure in the downstream region of the shock wave.

v_p (km/s)	v_s (km/s)	η	T (K)	P (GPa)
20	25.2	4.8	6 600	89
30	37.2	5.2	13 000	190
40	49.8	5.1	25 000	330
50	62.7	4.9	68 000	510
70	88.5	4.8	140 000	1000

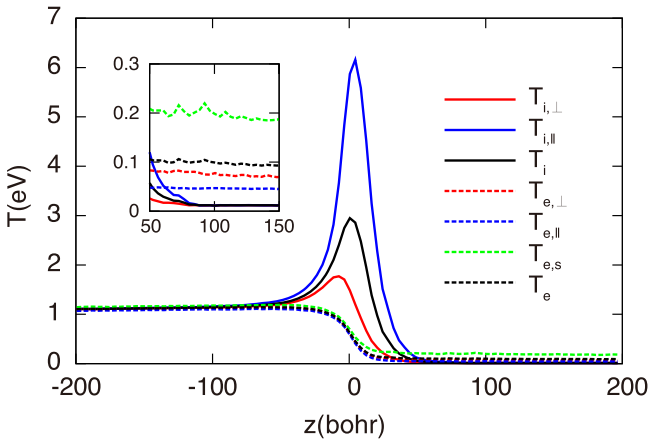

FIG. 1. Profiles of temperature components along the z axis for $v_p = 30\,\mathrm{km/s}$. They represent typical temperature distributions of strong shock waves. The inset is the zoom-in of temperature components in the upstream region.

interaction will lead to an overestimation to charge separation, but will not change the qualitative physical picture.

Profiles of macroscopic flow variables, such as temperature, density, and electrical field, are calculated in the coordinate systems moving with the shock front. Their values presented in this work are the spatial average in small slices of 4 bohr thickness along the z axis [17].

A quantity that one needs to pay special attention to is the electronic temperature T_e, which is derived from the wave-packet form of the wave function. In principle, it is defined as [37]

$$T_e = \frac{1}{4Nk_B}\sum_{\alpha}^{N} m_e\left(\mathbf{v}_{x,\alpha}^2 + \frac{3}{4}v_{s,\alpha}^2\right), \tag{3}$$

where N is the number of electrons in the calculation slice, and k_B is the Boltzmann constant. $\mathbf{v}_x$ and v_s represent $\dot{\mathbf{x}}$ and $\dot{s}$, respectively. The subscript α denotes the αth electron in the calculation slice. The s component of T_e is denoted as $T_{e,s}$, which is the second part of the summation in Eq. (3). Note that T_e approaches the real electronic temperature only at high temperature. At low temperature, e.g., in the initial state, when most electrons are in bound states, T_e calculated from Eq. (3) will essentially deviate from the real value, and thus can not be interpreted quantitatively.

III. RESULTS AND DISCUSSIONS

A. Structure of shock fronts

With the eFF method, one can have an atomic resolution for the fine structure of shock fronts, which, by taking electrons into consideration, displays different features compared with those revealed by classical MD method [11,17,24] or by other nonequilibrium methods [13,23,44] that do not take electronic excitation into consideration.

An important feature of the shock front structure is the strong "overshoot" [44], i.e., a high peak, of ion temperature and its components near the shock front, which is much weaker in the classical MD simulations [11,17,18]. Figure 1 shows the distributions of all temperature components near the shock front, including those of the ion temperature T_i, electron temperature T_e, as well as their components $T_{i,\parallel}$, $T_{i,\perp}$, $T_{e,\parallel}$, $T_{e,\perp}$, and $T_{e,s}$.

The ion temperature and its components have a protruding high peak at the shock front. It is a typical nonequilibrium phenomenon associated with the relaxation of ions [4]. Classical MD simulations have shown that [11,17,18] only $T_{i,\parallel}$ in a one-component medium has a perceivable "overshoot" near the shock front. However, Fig. 1 shows that $T_{i,\perp}$ also displays a significant "overshoot" in addition to $T_{i,\parallel}$. The peak of $T_{i,\parallel}$ is about 6 times the $T_{i,\parallel}$'s value in the downstream region far from the shock front. This ratio is much larger than that (1.5 times) observed in the classical MD simulations [17]. It suggests that, in addition to the kinetic relaxation revealed by MD simulations [11,17,18], there is an extra relaxation process taking place on both the parallel and perpendicular directions (with respect to the traveling direction of shock wave.) This extra relaxation process is attributed to the bond-breaking process of D-D bonds, as will be further discussed in Sec. III C.

The transition of electron temperature and its various components at the shock front is much smoother than that of ion temperatures. No "overshoot" is observed in either of them. The difference between the distributions of T_i and T_e is originated from the much smaller mass of electrons (0.01 amu in the simulation) compared with that of a deuterium atom. Roughly speaking, the relaxation time of an ensemble of particles is proportional to the square root of their mass, as estimated from the classical theory of plasmas [4]. This means that the relaxation process of electrons is about 10 times faster than that of ions, and thus difficult to observe in the transition region at a spatial resolution of 4 bohr.

The upstream region of the shock front is enlarged in the inset of Fig. 1. It shows that the value of all components of T_e in the upstream region is much higher than the components of T_i, which is 20 K in the simulation. This is not surprising since T_e has a quantum-mechanical origin, and it should be taken into account when interpreting the data quantitatively.

Velocity distributions of ions at various positions with respect to the shock front are displayed in Fig. 2. The distribution of the $v_\parallel$ component is similar to that revealed by classical MD simulations [11,17], whereas the distribution of $v_\perp$ shows a slightly different feature corresponding to the overshoot of $T_{i,\perp}$. As displayed in the inset of Fig. 2(a), the height of peaks in the $v_\perp$ distribution keeps increasing when the observing position in the downstream region leaves the shock front. In a Maxwellian velocity distribution, the increase of peak height corresponds to a decrease in temperature. This increasing trend displayed in $v_\perp$ thus corresponds to the drop of ion temperature at the rear of the shock front, which is in line with the relaxation of the "overshoot" in $T_{i,\perp}$, as displayed in Fig. 1.

B. Charge separation

With the eFF method, charge separation at the shock front can be illustrated in the dynamical simulations. When deuterium atoms are ionized, part of the bound electrons become free electrons. They have a larger translational thermal velocity than that of ions because $m_e \ll m_i$, and thus have a longer thermal diffusion length that can penetrate deeper into

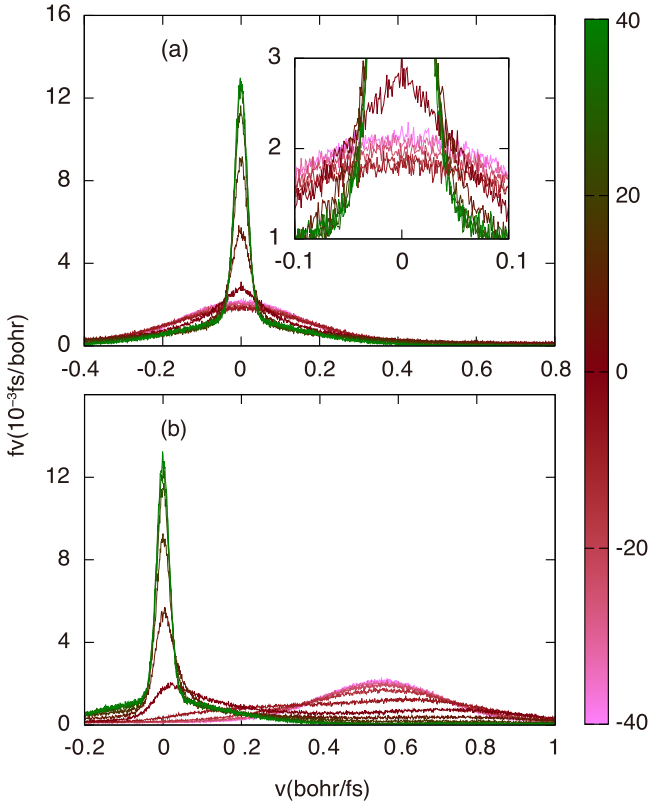

FIG. 2. Ion velocity distributions at selected positions near the shock front, in the simulation with a piston velocity $v_p = 30\,\mathrm{km/s}$. The color of each curve represents the distance with respect to the center of the shock front, as denoted by the color bar on the right side. (a) Velocity distribution on the perpendicular direction, and (b) the same as (a) but on the parallel direction, with respect to the propagation direction of shock waves. Positive distance in the color bar refers to location where the shock wave has not yet reached.

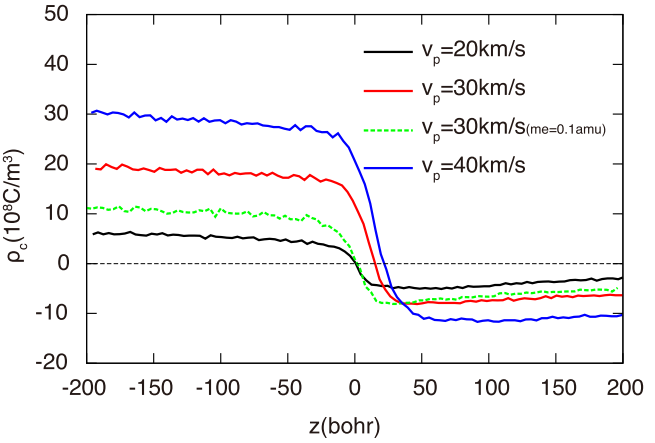

FIG. 3. Profiles of net charge density along the z axis for different piston velocities and electron masses. The black, red, and blue solid lines correspond to $v_p = 20$, 30, and 40 km/s and $m_e = 0.01$ amu, while the green dashed curve corresponds to $v_p = 30\,\mathrm{km/s}$ and $m_e = 0.1$ amu.

the upstream region (when observed in a reference framework moving with the shock front.) When a considerable number of ionized electrons penetrate the shock front, which leave ions with positive charges behind in the downstream region, a region of nonvanishing net charge density emerges near the shock front. As displayed in Fig. 3, negative charges are concentrated in the upstream region and positive charges are in the downstream region.

The influence of m_e can be further illustrated by setting m_e to be 0.1 amu. As displayed by the green dashed curve in Fig. 3, a significantly lower degree of charge separation can be observed, compared with the simulation with $m_e = 0.01$ amu, while both have the same piston velocity of $v_p = 30\,\mathrm{km/s}$. The accumulation of net charges in the downstream region is in contrast to the traditional picture of charge separation near the shock front, in which a localized ion-electron dipole layer at the shock front is formed [4,27], and the thickness of the dipole layer is of the same order of the shock front thickness. The picture of localized charge separation is important to most of the radiative hydrodynamic programs [15,16], in which the charge separation is entirely neglected because its spatial extension is considered much less than the resolution of the simulation grids. Our results are quite unexpected at first glance. It turns out to result from the lack of electron supplies at the downstream region of the shock front, where an impenetrable reflective piston is used. It keeps electrons from moving across the piston. Electrons which leave the downstream region with a speed higher than the average material speed then cannot find other sources of electrons to fill the space.

Whether the accumulation of net charges represents a real experimental situation depends on the setup of experiments. In gas gun experiments [45,46], the downstream flow can get electron supplies from the environment, e.g., the wall of the container. There is no problem to maintain the charge neutrality on large scales. However, in a typical implosion experiment [47], where the fuel parcel is driven by x-ray radiations, the downstream flow of the shock wave does not get external electron supplies when fast ionized electrons move inward to the center of the fuel parcel, as long as there is no convective instability driven by the strong electric field (induced by the net charges.)

A direct consequence for the accumulation of net charges is that it costs extra energy, which decreases the energetic efficiency of the driver. Since a relatively small cutoff of 10 bohr is used to calculate the interaction between particles in our simulation, where the long-range part of the Coulomb interaction is neglected, Fig. 3 provides an overestimated accumulation, and can thus only be used as a qualitative demonstration. A more accurate estimation of this effect in ICF is beyond the scope of the current work. It might be done with the simulation techniques that include a faithful description of the excited electrons as well as the coupling between radiative field and hot dense plasmas [40].

C. Molecular dissociation and ionization at the shock front

With the eFF method, dissociation of chemical bonds is clearly displayed. Figure 4 shows the radial distribution function (RDF) $g(r)$ of ions at various positions with respect to the shock front for $v_p = 20\,\mathrm{km/s}$ and $v_p = 30\,\mathrm{km/s}$. RDFs in front of the shock wave are presented as green curves,

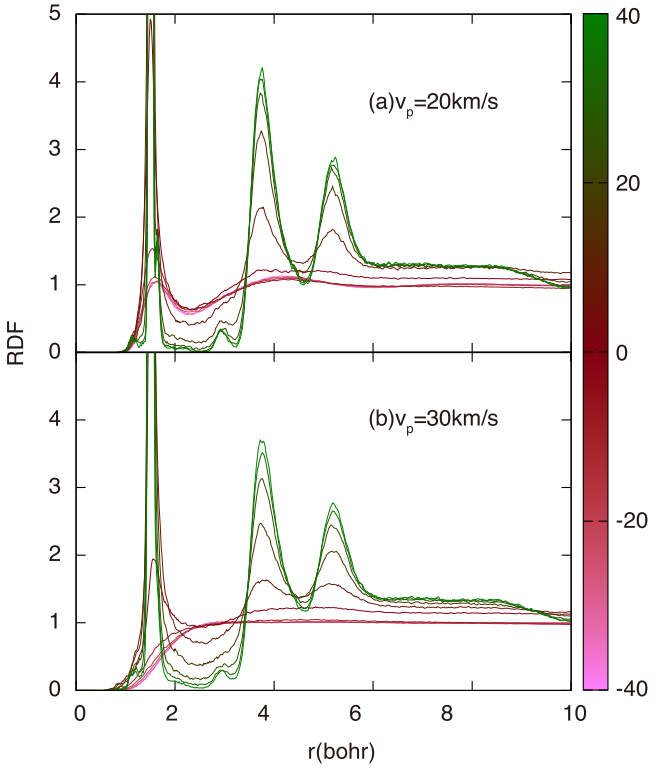

FIG. 4. Radial distribution functions at selected positions along the propagating direction of shock waves. The color of each curve corresponds to its distance from the center of the shock front, which is denoted in the color bar on the right side. Two cases are displayed corresponding to different piston velocities. In (a), $v_p = 20\,\mathrm{km/s}$, and in (b) $v_p = 30\,\mathrm{km/s}$. Positive distance in the color bar refers to location where the shock wave has not yet reached.

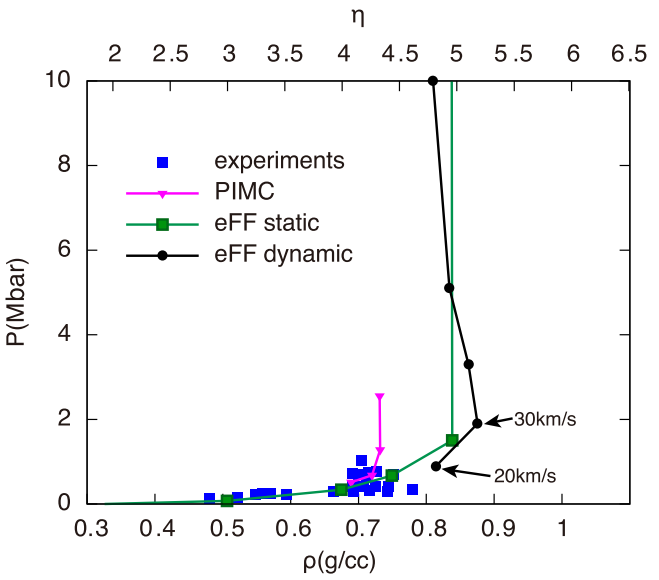

FIG. 5. Principal Hugoniot calculated in the eFF "dynamic" simulations of shock propagation, compared with those obtained from other approaches. The two arrows indicate the two states corresponding to $v_p = 20\,\mathrm{km/s}$ and $v_p = 30\,\mathrm{km/s}$. Results from the eFF method through the Rankine-Hugoniot relation are taken from [37], experimental results are taken from [45,50,51], and the PIMC results are from [29].

while those at the rear are displayed as pink lines. The first peak of the RDF in Fig. 4, located at $r \sim 1.4$ bohr (0.74 Å), corresponds to the D-D bond of D_2 molecules. The RDF also displays two additional peaks at larger r (∼3.7 and ∼5.2 bohr) in the upstream region of the shock front. They are attributed to the atoms of the nearest molecules. The peaks corresponding to the next-nearest molecules disappear in the RDF, which indicates that the initial state has a liquid structure. The height of the peaks decreases along with the shock transition, showing that a phase transition takes place at the shock front.

The height of the first peak is also a qualitative measurement of molecular dissociation. For both cases displayed in Fig. 4, the height of the first peak is significantly changed when the observing position crosses the shock front. In addition to that, also observed is the broadening of the peak width resulted from the increase of temperature. At positions away from the shock front, the height of the first peak is nearly a constant, which suggests that the dissociation of D_2 molecules takes place in the transient region near the shock front, and is synchronized with the passage of the shock wave. Although fast ionized electrons arrive before the shock front, as illustrated by the charge density profile in Fig. 3, they do not cause recognizable dissociation of D_2. This shows that the dissociation is essentially resulted from the kinetic effect of ion collisions. The impact of electrons has a small influence on the breaking of D-D bonds.

The first peak of $g(r)$ in the downstream region disappears between $v_p = 20\,\mathrm{km/s}$ and $v_p = 30\,\mathrm{km/s}$, as can been seen by comparing Figs. 4(a) and 4(b). These two states are also indicated with arrows in the principal Hugoniot in Fig. 5. It shows that these two states are located near the maximum compression ratio of the principal Hugoniot. This gives a strong support to the physical picture that the dissociation of D_2 molecules is the origin of the "bump" in the deuterium Hugoniot. Usually, the "bump" structure in the principal Hugoniot is the result of ionization of multishell electrons [48,49]. However, it has a slightly different origin in the principal Hugoniot curve of D_2.

Ionization requires higher energy than molecular dissociation in most cases. So, the ionization ratio is expected to be much smaller than that of the molecular dissociation. The number of ionized atoms in each calculation slice is estimated through $N_{\mathrm{ionized}} = N_l + N_c$, which has taken into consideration the fact that a portion of ionized electrons escape from the downstream to the upstream region of the shock front. Here, N_{ionized} is the number of ionized atoms, and N_l is the number of electrons for which the size parameter s is larger than a threshold r_c. $N_c = N_i - N_e$ is the number of net charges in the slice. The ionization ratio α is then calculated as $\alpha = N_{\mathrm{ionized}}/N_i$. In our calculations, r_c is chosen as 50 bohr, which is half of the length of the simulation box along the x and y axis, as suggested in [37]. Note that the absolute value of α depends on the choice of r_c, and might not be the same as in the measurement. Nevertheless, it provides a reasonable physical picture for the ionization of deuterium under shock impact.

The profiles of α for a variety of shock strengths are displayed in Fig. 6. The average ionization ratios are 3%,

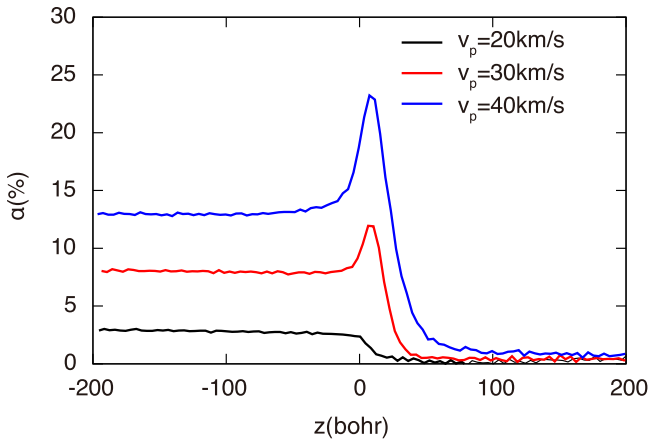

FIG. 6. Ionization ratio profiles along the propagating direction of shock waves. Profiles of different color correspond to different piston velocities, as indicated in the legend.

8%, and 13% corresponding to piston velocities of 20, 30, and 40 km/s. Note that at $v_p = 30$ km/s, most of the D_2 molecules are dissociated, whereas only 8% are ionized, which is a small fraction of the atoms. This shows that ionization is not a main source of the "bump" structure in the principal Hugoniot curve of D_2. It is also noticed that there is a peak of α in the transition region of shock front, which corresponds to an "overshoot" of the ionization and its recovering process. The similarity of this peak structure with that of T_i displayed in Fig. 1 suggests that the ionization at the shock front is induced by the kinetics of ions.

D. Principal Hugoniot from dynamical simulations

There have been extensive efforts [21,29,45,50–54] to measure and calculate the principal Hugoniot of D_2, which serves as a major benchmark for various equations of state (EOS) used in ICF. Experimentally, the high energy density state is generated by driving a shock wave in the sample materials using gas guns [22,45], exploding wires [50,51] or lasers [21,52], which is similar to the setup used in the dynamical simulations. On the other hand, there are a number of theoretical methods [29,53,54] which estimate the principal Hugoniot of D_2 via the Rankine-Hugoniot relation [4]. Reproducing the principal Hugoniot in a dynamical way provides a direct evaluation to the accuracy and validity of the eFF method.

In Fig. 5, the solid circular dots represent the Hugoniot curve estimated from the dynamical simulations with the eFF method. It is compared with the Hugoniot calculated with the same method but through the Rankine-Hugoniot relation [37], displayed as square dots. The comparison shows that these two Hugoniots agree reasonably well with each other. So, there is no fundamental obstacle to apply the eFF method in the simulation of a highly nonequilibrium process. Note that the Hugoniot in Fig. 5 is simulated with $m_e = 0.01$ amu, whereas the result through the Rankine-Hugoniot relation is calculated with $m_e = 1$ amu. These results show that reducing the mass of electrons does not change the equilibrium property of D_2 in the downstream region of the shock front.

Also displayed are typical experimental measurements conducted in recent years [45,50,51] together with results of the path-integral Monte Carlo (PIMC) method [29]. They show that the largest compression ratio of D_2 is ~4.3, whereas the eFF gives a slightly overestimated prediction of ~5.2. This deviation is associated with the underestimation of the dissociation energy in the eFF method (67.2 kcal/mol for the eFF method and 104.2 kcal/mol for the exact bonding energy) [37], which makes the material easier to compress.

IV. SUMMARY

In summary, a systematic study of shock wave propagating in dense deuterium is carried out with the eFF method. Several nonequilibrium features associated with the excitation of electrons near the shock front are displayed, which afford a more complicated shock wave structure compared with the structure revealed by the methods that do not consider the effect of electrons. The physical picture provided by the simulation could be helpful to build a more realistic picture of shock wave propagation in fuel materials commonly used in ICF.

ACKNOWLEDGMENTS

This work is financially supported by the Science Challenge Project (Grant No. JCKY2016212A501), NSFC (Grant No. 11274019), and NSAF (Grant No. U1530113). Part of the calculations were supported by the Special Program for Applied Research on Super Computation of the NSFC-Guangdong Joint Fund (the second phase).

[1] S. Nakai and H. Takabe, Rep. Prog. Phys. **59**, 1071 (1996).
[2] J. Lindl, Phys. Plasmas **2**, 3933 (1995).
[3] X. He, J. Li, Z. Fan, L. Wang, J. Liu, K. Lan, J. Wu, and W. Ye, Phys. Plasmas **23**, 082706 (2016).
[4] Y. B. Zeldovich and Y. P. Raizer, *Physics of Shock Waves and High-Temperature Hydrodynamic Phenomena*, edited by W. D. Hayes and R. F. Probstein (Academic Press, New York, 1967).
[5] C. Muckenfuss, Phys. Fluids **5**, 1325 (1962).
[6] V. Y. Klimenko and A. N. Dremin, *Detonatsiya, Chernogolovka*, edited by O. N. Breusov (Akademik Nauk, Moscow, 1978).
[7] B. L. Holian and G. K. Straub, Phys. Rev. Lett. **43**, 1598 (1979).
[8] B. L. Holian, Shock Waves **5**, 149 (1995).
[9] W. G. Hoover, Phys. Rev. Lett. **42**, 1531 (1979).
[10] W. G. Hoover and C. G. Hoover, arXiv:0909.2882.
[11] V. Zhakhovskii, K. Nishihara, and S. Anisimov, J. Exp. Theor. Phys. **66**, 99 (1997).
[12] V. V. Zhakhovskii, S. V. Zybin, K. Nishihara, and S. I. Anisimov, Phys. Rev. Lett. **83**, 1175 (1999).
[13] C. Lin, A. Xu, G. Zhang, Y. Li, and S. Succi, Phys. Rev. E **89**, 013307 (2014).

[14] H. M. Mott-Smith, Phys. Rev. **82**, 885 (1951).
[15] R. Ramis, R. Schmalz, and J. Meyer-ter Vehn, Comput. Phys. Commun. **49**, 475 (1988).
[16] G. Zimmerman and W. Kruer, Comments Plasma Phys. Controlled Fusion **2**, 51 (1975).
[17] H. Liu, W. Kang, Q. Zhang, Y. Zhang, H. Duan, and X. T. He, Front. Phys. **11**, 115206 (2016).
[18] B. L. Holian, M. Mareschal, and R. Ravelo, J. Chem. Phys. **133**, (2010).
[19] A. B. Belonoshko, A. Rosengren, N. Skorodumova, S. Bastea, and B. Johansson, J. Chem. Phys. **122**, 124503 (2005).
[20] V. Fortov, R. Ilkaev, V. Arinin, V. Burtzev, V. Golubev, I. Iosilevskiy, V. Khrustalev, A. Mikhailov, M. Mochalov, V. Y. Ternovoi *et al.*, Phys. Rev. Lett. **99**, 185001 (2007).
[21] G. W. Collins, L. B. Da Silva, P. Celliers, D. M. Gold, M. E. Foord, R. J. Wallace, A. Ng, S. V. Weber, K. S. Budil, and R. Cauble, Science **281**, 1178 (1998).
[22] Q. Chen, L. Cai, Y. Gu, J. Zheng, and G. Ji, Phys. Lett. A **374**, 3875 (2010).
[23] L. García-Colín, R. Velasco, and F. Uribe, Phys. Rep. **465**, 149 (2008).
[24] B. L. Holian, C. W. Patterson, M. Mareschal, and E. Salomons, Phys. Rev. E **47**, R24(R) (1993).
[25] B. L. Holian and M. Mareschal, Phys. Rev. E **82**, 026707 (2010).
[26] J. T. Su and W. A. Goddard, Phys. Rev. Lett. **99**, 185003 (2007).
[27] M. A. Liberman and A. L. Velikovich, *Physics of Shock Waves in Gases and Plasmas*, Springer Series in Electrophysics, Vol. 19 (Springer-Verlag, Berlin/New York, 1986).
[28] M. A. Marques and E. Gross, Annu. Rev. Phys. Chem. **55**, 427 (2004).
[29] B. Militzer and D. M. Ceperley, Phys. Rev. Lett. **85**, 1890 (2000).
[30] N. D. Mermin, Phys. Rev. **137**, A1441 (1965).
[31] W. Kang, S. J. Zhao, S. Zhang, P. Zhang, Q. F. Chen, and X.-T. He, Sci. Rep. **6**, 20623 (2016).
[32] S. Zhao, W. Kang, J. Xue, X. Zhang, and P. Zhang, Phys. Lett. A **379**, 319 (2015).
[33] A. D. Baczewski, L. Shulenburger, M. P. Desjarlais, S. B. Hansen, and R. J. Magyar, Phys. Rev. Lett. **116**, 115004 (2016).
[34] M. Knaup, P.-G. Reinhard, and C. Toepffer, Contrib. Plasma Phys. **41**, 159 (2001).
[35] M. Knaup, P. Reinhard, C. Toepffer, and G. Zwicknagel, J. Phys. A Math. Gen. **36**, 6165 (2003).
[36] F. Graziani, M. P. Desjarlais, R. Redmer, and S. B. Trickey, *Frontiers and Challenges in Warm Dense Matter*, Vol. 96 (Springer Science & Business, Cham, Switzerland, 2014).
[37] J. T. Su, Ph.D. thesis, California Institute of Technology, 2007.
[38] J. T. Su and W. A. Goddard, J. Chem. Phys. **131**, 244501 (2009).
[39] A. Jaramillo-Botero, J. Su, A. Qi, and W. A. Goddard, J. Comput. Chem. **32**, 497 (2011).
[40] R. P. Drake, *High-Energy-Density Physics: Fundamentals, Inertial Fusion, and Experimental Astrophysics* (Springer Science & Business Media, Berlin/Heidelberg, 2006).
[41] R. L. Liboff, *Introduction to Quantum Mechanics* (Addison-Westley, Reading, 1980).
[42] E. J. Heller, J. Chem. Phys. **62**, 1544 (1975).
[43] S. Plimpton, J. Comput. Phys. **117**, 1 (1995), http://lammps.sandia.gov.
[44] S.-M. Yen, Phys. Fluids **9**, 1417 (1966).
[45] N. C. Holmes, M. Ross, and W. J. Nellis, Phys. Rev. B **52**, 15835 (1995).
[46] Y. Gu, Q. Chen, L. Cai, Z. Chen, J. Zheng, and F. Jing, J. Chem. Phys. **130**, 184506 (2009).
[47] J. D. Lindl, P. Amendt, R. L. Berger, S. G. Glendinning, S. H. Glenzer, S. W. Haan, R. L. Kauffman, O. L. Landen, and L. J. Suter, Phys. Plasmas **11**, 339 (2004).
[48] S. Zhang, H. Wang, W. Kang, P. Zhang, and X. T. He, Phys. Plasmas **23**, 042707 (2016).
[49] B. F. Rozsnyai, J. R. Albritton, D. A. Young, V. N. Sonnad, and D. A. Liberman, Phys. Lett. A **291**, 226 (2001).
[50] M. D. Knudson, D. L. Hanson, J. E. Bailey, C. A. Hall, J. R. Asay, and W. W. Anderson, Phys. Rev. Lett. **87**, 225501 (2001).
[51] M. D. Knudson, D. L. Hanson, J. E. Bailey, C. A. Hall, and J. R. Asay, Phys. Rev. Lett. **90**, 035505 (2003).
[52] L. B. Da Silva, P. Celliers, G. W. Collins, K. S. Budil, N. C. Holmes, T. W. Barbee Jr., B. A. Hammel, J. D. Kilkenny, R. J. Wallace, M. Ross, R. Cauble, A. Ng, and G. Chiu, Phys. Rev. Lett. **78**, 483 (1997).
[53] C. Pierleoni, D. M. Ceperley, B. Bernu, and W. R. Magro, Phys. Rev. Lett. **73**, 2145 (1994).
[54] T. J. Lenosky, S. R. Bickham, J. D. Kress, and L. A. Collins, Phys. Rev. B **61**, 1 (2000).